

Formation and annealing of defects during high-temperature processing of ion-implanted epitaxial silicon: the role of dopant implants

P.K. Giri ^a, G. Galvagno ^a, A. La Ferla ^a, E. Rimini ^{a,*}, S. Coffa ^b, V. Raineri ^b

^a *Dipartimento di Fisica, Università di Catania, 57 Corso Italia, 195129 Catania, Italy*

^b *CNR-IMETEM, 50 Stradale Primosele, 195121 Catania, Italy*

Abstract

We have investigated the optical and structural characteristics of defect evolution during high-temperature annealing of keV-ion-implanted epitaxial silicon using optical microscopy (OM), photoluminescence (PL) spectroscopy and transmission electron microscopy (TEM). Postimplantation annealing in oxygen ambient resulted in oxidation-induced stacking faults (OISFs) and dislocations. The PL spectrum of these samples is dominated primarily by a dislocation-related D1 line, which is particularly strong in Al-implanted samples as a consequence of the enhanced formation of dislocations with Al implantation. Comparative analysis of the PL signature and OM observations of defects for different implants suggests that D1 and D2 lines result from dislocations rather than in the OISFs. Indeed, it is found that OISFs act as a nonradiative recombination channel in the luminescence of Si. PL studies of N₂-annealed samples indicate the formation of nonradiative defect centres. In the case of dopant implants, after rapid thermal annealing (RTA) for 2 min in N₂ ambient, the specific signature of extended defects was found from PL studies, while TEM analysis reveals the presence of <111> precipitates located in a region with a high dislocation density. In comparison with other dopants, Al implants show an enhanced formation of extended defects, and they are found even at a depth beyond the end-of-ion range damage. © 2000 Published by Elsevier Science S.A. All rights reserved.

Keywords: Extended defects; Implantation; Photoluminescence; Precipitates; Annealing; TEM

1. Introduction

With the stringent requirements for the optimum processing of modern-generation semiconductor devices, it is imperative to understand the nature and origin of process-induced defects in silicon (Si) [1,2]. Despite several decades of studies of defects due to ion implantation, particularly with dopant ions in Si, a thorough understanding of several unwanted phenomena such as impurity precipitation, out-diffusion, segregation, low electrical activation, etc., during semiconductor processing is lacking in the literature [3]. In particular, compared to other dopants in Si, Al doping is known to exhibit anomalous behavior in terms of the phenomena mentioned above. However, little is known about the role of processing steps and

implant-induced defects in the manifestation of such behavior [4,5].

It is known that high dose implantation-induced defects can act as a nucleation site for the formation and evolution of defects during post-implantation processing. High-temperature annealing, and in particular, rapid thermal annealing, is routinely adopted in semiconductor processing to achieve dopant activation and damage removal while leaving unwanted diffusion. However, the role of secondary defects resulting from such processes have been investigated to a lesser extent [6]. The precipitation of impurities above the solid solubility limit has been extensively studied in the literature, but the detailed role of processing steps, the impact of implant-induced defects and damage on dopant precipitation below the solid solubility limit is not well understood [7].

Photoluminescence (PL) spectroscopy is a sensitive tool to study the radiative recombination properties of various defects in Si [8]. While most of the studies have

* Corresponding author. Tel.: +39-95-7195418; fax: +39-95-3830238.

E-mail address: rimini@ct.infn.it (E. Rimini)

focused on common impurity-related PL signature in Si, a proper understanding of the origin of PL in various extended defects in Si is lacking in the literature. Among the various extended defects, oxidation-induced stacking faults (OISFs) and dislocations have been the subjects of extensive investigations in the past using various tools. However, there exists a debate about the origin of PL D lines in Si containing dislocation and OISFs [9] — while it is commonly believed that dislocations decorated with impurities result in D1 and D2 PL lines from Si [10]. Similar conclusions have been drawn from the analysis of electronic and optical properties of OISFs [11].

This work is aimed at investigating the optical and structural characteristics of various defects that evolve during high-temperature annealing of ion implanted Si. The defects have been characterized using PL, cross-sectional-transmission electron microscopy (XTEM), and optical microscopy (OM); this was after chemical etching to understand the role of implant species and annealing ambient in extended defect nucleation, growth and dissolution during standard technological processes. Studies of OISFs and dislocations, using complementary techniques, provide important informa-

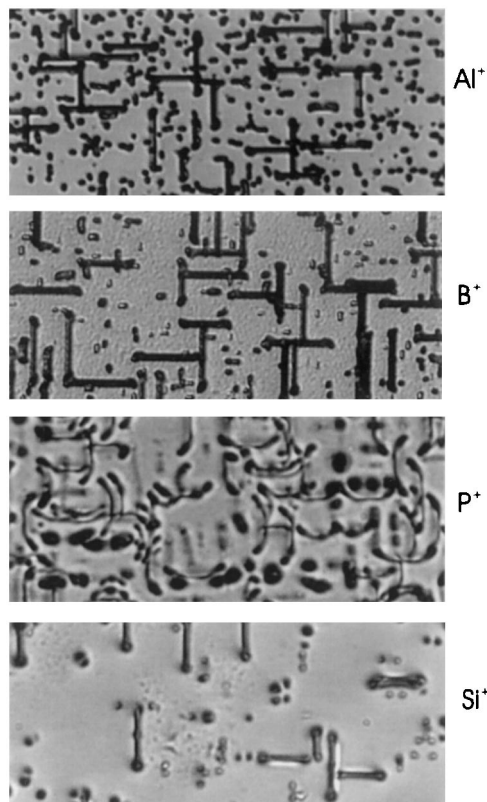


Fig. 1. Optical-microscopy image of Schimmel-etched Si wafers subjected to implantation with different ion species (Al⁺, B⁺, P⁺, Si⁺) and subsequent oxidation at 1200°C for 1 h in dry oxygen. A magnification of 500 is used to show the presence of dislocations (dots) and OISFs (lines).

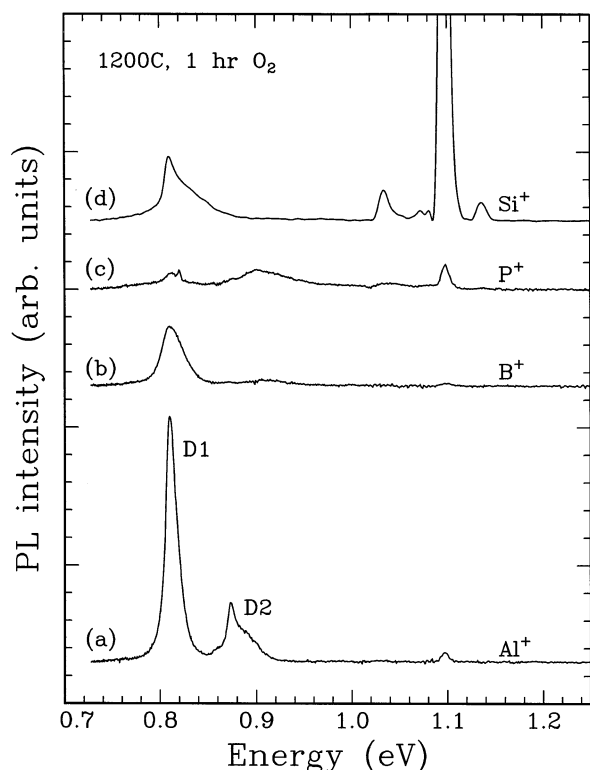


Fig. 2. Comparison of PL spectra at 17 K for Si implanted with different ion species (Al⁺, B⁺, P⁺, and Si⁺), and subsequently oxidized at 1200°C for 1 h in dry oxygen. D1 and D2 refer to well-known dislocation-related PL lines in Si.

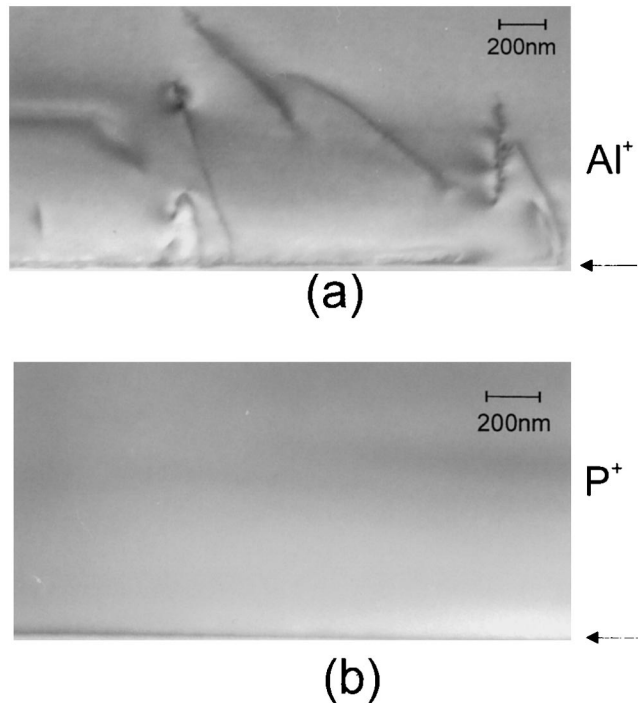


Fig. 3. Cross-sectional TEM image of extended defects for (a) Al and (b) P implanted Si after O₂ annealing. A high density of dislocation lines is clearly seen in the Al⁺-implanted case. The arrow indicates the location of the surface.

tion about the origin of D lines in the PL spectrum. We provide spectroscopic evidence of dopant precipitation during the rapid thermal annealing of implanted Si, even for concentrations below the solid solubility limit. Different sources of extended defects in thermally pro-

cessed wafers have been investigated, and the specific behavior of Al in comparison with other conventional dopants and to self-ion-implanted Si is pointed out.

2. Experimental details

The experiments were performed on phosphorous-doped epitaxial (EPI) Si layers 60 μm thick ($\rho \approx 70 \Omega \text{ cm}$) grown on FZ Si wafers. The implantation of Al^+ , B^+ , P^+ , and Si^+ ions was made on an epitaxial layer at an energy of 80 keV and to a dose of $1 \times 10^{14} \text{ cm}^{-2}$. The implanted samples were oxidized with dry O_2 for 1 h at 1200°C on preannealed or as-implanted wafers. The preannealing of the implanted wafers was performed using rapid thermal annealing (RTA) for 30 s and 2 min, or furnace annealing for 1 h under N_2 flux (2 l min^{-1}) at a temperature of 1200°C . For furnace annealing, the samples were inserted sufficiently fast into the tube of the furnace, maintained at 1200°C , and taken out after 1 h without allowing extra time for slow heating or cooling. Two min of RTA was performed in four steps of 30 s each with an interval of a few min in-between for cooling. PL measurements were carried out at 17 K using a closed cycle He cryostat, and luminescence was excited using the 488 nm line of an Ar laser. The luminescence was analyzed using a CVI spectrometer with a single-grating monochromator. All oxidized specimens were etched in dilute HF solution to remove the oxide layer before performing PL measurements. For OM observation of extended defects, oxidized wafers were at first etched in hydrofluoric acid solution to remove the oxide layer, and subsequently etched for 30 s in Schimmel solution [12]. Defects and precipitates were also analyzed by XTEM. A JEOL 2010 transmission electron microscope operating at 200 kV was used for recording the image.

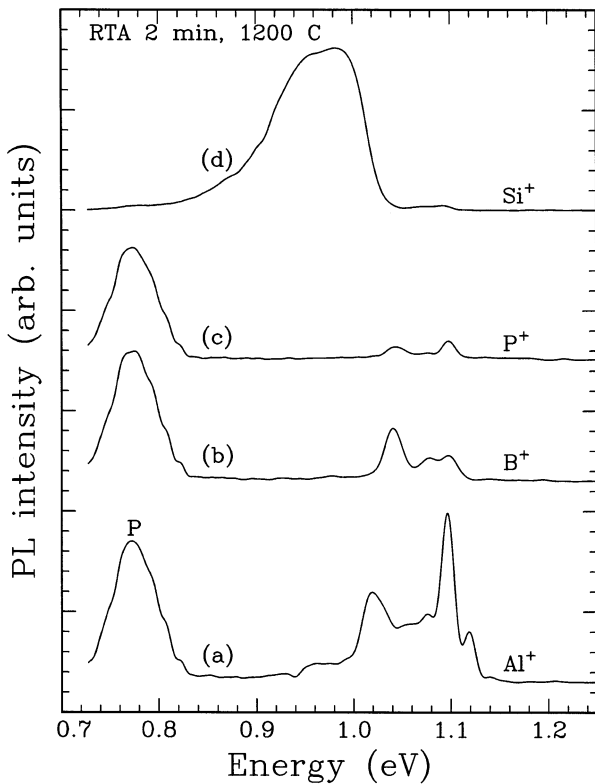


Fig. 4. PL spectra at 17 K of Si implanted with various ions and subsequently subjected to RTA for 2 min in N_2 : (a) Al^+ ; (b) B^+ ; (c) P^+ ; and (d) Si^+ . The broad peak P at $\approx 0.77 \text{ eV}$ is related to dopant precipitates.

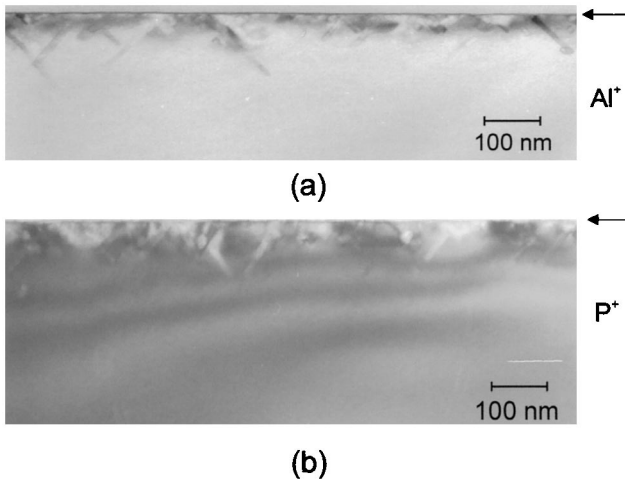


Fig. 5. Comparison of bright field XTEM images for Al^+ and P^+ implanted and subsequently RTA annealed (2 min, 1200°C) EPI Si. The Al^+ -implanted sample shows a high density of precipitates and dislocation lines at large depths. The arrow points to the location of the Si surface.

3. Results and discussion

3.1. Defect evolution under O_2 annealing

Fig. 1 shows a set of optical-microscopy images for various implanted wafers after subsequent annealing in dry O_2 at 1200°C for 1 h. The processed wafers were Schimmel etched for 30 s to delineate the defects in all samples except for P^+ -implanted Si, which was etched for a longer duration. For Al^+ -, B^+ -, and Si^+ -implanted wafers, a high density of OISFs ($\approx 10^6 \text{ cm}^{-2}$) and dislocations ($\approx 10^7 \text{ cm}^{-2}$) was observed, while the sample with P^+ implantation shows no OISFs. After etching (Schimmel) for 90 s, the P^+ -implanted sample shows a high density of epistacking faults, as shown in Fig. 1. It is also clear from Fig. 1 that the density of dislocations (dots) is high in the Al^+ -implanted sample

compared to other cases. The measured length ($\approx 12 \mu\text{m}$) of OISFs is as expected from calculations with known growth rates. However, a nonuniform size distribution in OISF lengths is indicative of the preferential growth of stacking faults in defect-nucleated regions. The density of OISFs is particularly low in the Si^+ -implanted case. The absence of OISFs in P^+ -implanted Si has been reported earlier, but no explanation is known [13]. The implanted wafers which were subjected to preannealing in N_2 ambient prior to oxidation show a reduced concentration of defects. However, samples subjected to 1200°C annealing for 1 h in N_2 showed a substantial amount of residual dislocation in Si^+ implanted samples, while Al^+ - and B^+ -implanted samples showed low concentrations of OISFs and dislocations. The presence of defects after such high thermal budget may imply that nucleation sites for extended defect formation were not completely annealed out, or defects introduced during N_2 annealing act as a nucleation site for such extended defects. Indeed, we found that virgin Si wafers that were subjected to preannealing in N_2 and subsequently oxidized showed the presence of OISFs in low density ($\approx 5 \times 10^4 \text{ cm}^{-2}$) irrespective of the preannealing time duration. Hence, residual defects in preannealed samples are partly because of contamination in the furnace/RTA chamber and thermal stress, particularly associated with the RTA process [7].

Fig. 2 shows a set of PL spectra recorded at 17 K for the same set of samples as used in Fig. 1, which were implanted and subsequently annealed in oxygen for 1 h at 1200°C . In the case of Al^+ -implanted Si, the spectrum is dominated by a sharp peak at 0.810 eV (labeled D1) and another relatively weak peak at 0.875 eV (labeled D2). The peak at 0.810 eV is common to all spectra in varying intensity, as a result of different implant species. However, apart from the Al^+ -implanted case, the 0.875 line intensity is negligible or absent in samples with other implant species. The peak at 0.810 eV is due to well known dislocation-related defects, commonly denoted as D1, and the peak at 0.875 eV is also ascribed to dislocation-related defects, referred to as D2 [10]. In the case of Si^+ implants, the D1 line is broad with a higher energy shoulder and the band-edge-related signal (at $\approx 1.12 \text{ eV}$) is very high, comparable to the PL signal from virgin Si. This latter feature in Si^+ -implanted samples indicates that sufficient damage recovery or annealing of the nonradiative channel has occurred during annealing in oxygen ambient. PL studies on preannealed (in N_2 ambient) and oxidized samples show a complete suppression of D lines. Moreover, neither was the TO phonon-related PL peak detectable in these sets of samples — in spite of the expected annealing of defects/damage during preannealing. This indicates that defects induced during preannealing act as a non-radiative channel to PL in Si.

Note that we observed, from OM studies on preannealed, oxidized specimens, a reduced concentration of OISFs and dislocations with an increasing annealing time. However, the residual defects are found to be nonradiative in Si.

Dislocation-related D1 and D2 lines have been extensively studied in literature and are believed to result from bound-to-bound transitions [10]. D1 and D2 lines have been reported to occur in ionimplanted Si, heat treated CZ Si, oxidation-induced stacking faults, etc. During the oxidation of Si, a large concentration of Si interstitials are injected into the Si matrix at the Si– SiO_2 interface because of the change in the volume ratio of Si and SiO_2 [14]. The lattice damage induced by ion implantation acts as a nucleation site for the formation of extended defects such as dislocations and stacking faults during the oxidation of Si. For common dopant implants, the formation of stacking faults and dislocation upon oxidation of Si has been widely studied [13], and it has been reported that the oxidation of phosphorus-implanted Si does not give rise to OISFs in Si, while it forms epistacking faults that lies deep in the bulk. It has also been reported that while chemical etching failed to delineate OISFs in a phosphorous-doped layer, TEM observations showed OISFs [15]. Therefore results from one technique need to be compared with those of other techniques. On the other hand, dislocation formation during annealing in O_2 is known to be common to all dopant implants and we observed corresponding D lines in PL spectra, as shown in Fig. 2.

A relatively strong D1 line in Al -implanted and oxidized Si indicates that dislocation and oxidation-induced stacking-fault formation were enhanced in this case in comparison to B and P dopants species. The optical images shown in Fig. 1 reveal that the dislocation density in the Al^+ -implanted sample is about two times that of the B^+ -implanted sample, while OISF density is similar in the two cases. Therefore, the stronger D1 line in PL spectra for the Si– Al^+ sample refers to the fact that the D1 line is more fundamental to dislocations than OISFs. A close look at Fig. 1 and Fig. 2 for P^+ -implanted samples reveals, rather, that OISFs act as a nonradiative channel for PL in Si. They cause suppression of band-edge-related signals in PL and the dislocations are responsible for the D1 line in the PL spectra of Si — contrary to the belief that OISFs give rise to D1 and D2 lines [11].

Fig. 3 shows the comparison of XTEM micrographs of Al^+ - and P^+ -implanted and subsequently oxygen-annealed wafers, showing clearly the high density of dislocation in the Al^+ -implanted sample. The dislocation lines extend to $\approx 1 \mu\text{m}$ while ion damage is located at about $0.1 \mu\text{m}$. Therefore, defects in Al^+ -implanted cases are formed very deep in the bulk, perhaps due to the high diffusivity of Al in Si. Furthermore, XTEM analysis of P^+ -implanted and oxidized Si showed no

detectable density of extended defects (Fig. 3(b)), including dislocations and stacking faults. This is correlated with the very weak D lines in the PL spectrum (see Fig. 2) for this sample and therefore the above conclusion relating to D1 and D2 lines is supported by such observations. From RTA annealing in N_2 , and subsequent oxidation of Al^+ -implanted wafers, we found further evidence that D1 and D2 lines cannot be correlated with OISFs, and that they are characteristics of dislocations only. Details of these results will be published elsewhere [16].

3.2. Defect evolution during preannealing under N_2

Fig. 4 shows PL spectra for Si samples implanted with Al^+ , B^+ , P^+ and Si^+ ions in equal doses ($1 \times 10^{14} \text{ cm}^{-2}$) and RTA processed for 2 min at 1200°C in N_2 ambient. The peak labeled P at $\approx 0.77 \text{ eV}$ is common to all dopant implants, while Si^+ -implanted samples show a broader peak at higher energy, as seen in curve (d) of Fig. 4. During annealing in N_2 ambient, the peak P evolves with RTA of 2 min and reduces substantially after annealing for 1 h. The occurrence of the broad peak in PL spectra is often related to the presence of macrodefects such as defect clusters in the crystalline matrix [17], and a model has been proposed in the literature for such broad PL peaks, taking into account the quantum confinement of carriers in the strained region of the lattice caused by ion damage [18]. In the present case, we believe that the implanted dopant atoms form precipitates in the damaged region during the high-temperature RTA process and the broad peak P results from strain surrounding these precipitates. The solid solubility limit at 1200°C for different implanted dopants used in this work is much higher compared to the maximum concentration of dopants in the implanted peak region. For example, the peak concentration of implanted Al is found to be $\approx 3.7 \times 10^{18} \text{ cm}^{-3}$ (using secondary ion mass spectrometry) whereas the solubility limit is $\approx 2 \times 10^{19} \text{ cm}^{-3}$. For B and P, the solid solubility limit at this temperature is 5×10^{20} and $1.4 \times 10^{21} \text{ cm}^{-3}$, respectively. Although maximum concentrations of the implanted dopants are well below the solid solubility limit, in the present case the thermal nonequilibrium condition resulting from the use of a high ramp rate during annealing is most likely to be responsible for such precipitation. Another important factor contributing to the precipitation process is the fast diffusion of dopants in the nearly amorphous layer of damaged Si and the corresponding precipitation at the amorphous–crystalline interface during RTA [8].

The structure of the defects in these RTA annealed samples was further investigated by TEM analysis. Fig. 5 shows bright-field XTEM images of Al^+ - and P^+ -implanted Si and RTA (2 min)-annealed Si. The presence

of precipitates and dislocations near the surface is clearly seen in both the cases. Compared to the P^+ -implanted sample, the Al^+ -implanted sample shows dislocation lines, and the precipitates are located exactly at these dislocations [19]. This may indicate that Al trapping in dislocation is responsible for efficient precipitation, even below the solid solubility limit [20]. The dislocation lines were found to be extended to a relatively deeper region in the case of Al^+ -implanted samples, because of their high diffusivity. The precipitates were found to be $\langle 111 \rangle$ oriented in both cases. In spite of the presence of dislocations in these samples, we did not observe any D-line luminescence in the PL spectra of Fig. 4. It might indicate that the presence of precipitates acts as a nonradiative channel for D-line luminescence.

The occurrence of the broad peak P (at $\approx 0.77 \text{ eV}$) in PL spectra with similar intensity for all three dopant implants indicates similar efficiency of precipitation process independent of the dopant species. However, the peak was shifted to higher energy and broadened for Si implants and subsequent RTA. Si implantation gave rise to excess Si interstitials of large concentrations for the $1 \times 10^{14} \text{ cm}^{-2}$ Si^+ dose, and the extended interstitial chains are expected to form in such a high dose limit. The interstitial diffusivity is known to be very high even at RT, which is consistent with their fast migration and extended defect formation. However, the RTA produces a distribution of these defects such that they experience an inhomogeneous environment and this is believed to result in a relatively broad peak. For higher-temperature annealing these defect chains may align to produce $\{311\}$ defects which are primarily due to interstitial clustering [21]. We believe that the broad peak in self-implanted Si results from interstitial chains of relatively small size. It is important to mention here that XTEM analysis of Si^+ implanted RTA annealed samples did not show any detectable extended defects, in contrast to dopant-implanted cases. Studies on microdefect formation during annealing has revealed the signature of a broad PL peak related to Si interstitials [17]. We have observed that this peak in PL appears in a smaller intensity (not shown) for samples annealed for 1 h at 1200°C in N_2 . As this thermal budget is high enough to recover damage and dissociate any clusters from more stable extended defects, the exact nature of these defects in the Si^+ -implanted case remains unclear and needs further investigation.

4. Conclusions

Using optical and structural characterization, extended-defect formation and their evolution during the thermal annealing of keV-implanted epitaxial Si has been investigated for various implanted ion species. It is

shown that annealing in N₂ ambient gives rise to defects which are different from those that form during annealing in O₂ ambient. Oxygen annealing of implanted wafers results in dislocations and oxidation-induced stacking faults at high concentration in the case of Al implants. The results of optical microscopy, TEM and PL have been correlated and it is concluded that D-line luminescence in PL spectra is due to dislocations. Contrary to the idea that OISFs give rise to D1 and D2 lines in PL, our results indicate their non-radiative nature in Si. We have provided spectroscopic evidence of dopant precipitation during RTA of implanted dopant ions, even at a concentration below the solid solubility limit, which has been explained on the basis of fast diffusion of dopants in the damaged region and trapping by extended defects. XTEM analysis of dopant-implanted Si showed <111> oriented precipitates in N₂ RTA-annealed Si, while no defects were detectable for Si⁺-implanted Si.

Acknowledgements

We are thankful to A. Marino, M. Furnari and S. Panniteri for their expert technical assistance in sample preparation. One of the authors (P.K. Giri) gratefully acknowledges the research-fellowship grant from ICTP, Trieste under the TRIL programme.

References

- [1] C. Claeys, E. Simoen, J. Vanhellemont, Nucl. Instr. A 377 (1996) 244.
- [2] G. Kissinger, D. Graf, U. Lambert, T. Grabolla, H. Richter, Semicod. Sci. Technol. 12 (1997) 933.
- [3] A. Claverie, L.F. Giles, M. Omri, B. de Mauduit, G. Ben Assayag, D. Mathiot, Nucl. Instr. Methods Phys. Res. B 147 (1999) 1.
- [4] G. Galvagno, F. La Via, F. Priolo, E. Rimini, Semicod. Sci. Technol. 8 (1993) 488.
- [5] G. Galvagno, A. Scandurra, V. Raineri, et al., J. Electrochem. Soc. 140 (1993) 2313.
- [6] E. Susi, A. Poggi, M. Madrigali, J. Electrochem. Soc. 142 (1995) 2081.
- [7] O.W. Holland, J. Narayan, D. Fathy, S.R. Wilson, J. Appl. Phys. 59 (1986) 905.
- [8] G. Davies, Phys. Rep. 176 (1989) 83.
- [9] V. Higgs, M. Goulding, A. Brinklow, P. Kightley, Appl. Phys. Lett. 60 (1992) 1369.
- [10] R. Sauer, J. Weber, J. Stolz, E.R. Weber, K.-H. Kusters, H. Alexander, Appl. Phys. A 36 (1985) 1, and references therein.
- [11] J.H. Evans, J. Kaniewski, M. Kaniewska, J.S. Rimmer, Semicod. Sci. Technol. 7 (1992) A41.
- [12] D.G. Schimmel, J. Electrochem. Soc. 126 (1979) 479.
- [13] S. Prussin, J. Appl. Phys. 45 (1974) 1635.
- [14] S.M. Hu, Mater. Sci. Eng. R 13 (1994) 105.
- [15] Kenji Nishi, D.A. Antoniadis, J. Appl. Phys. 56 (1984) 3428.
- [16] P.K. Giri, S. Coffa, V. Raineri, G. Galvagno, A. La Ferla, E. Rimini, Unpublished.
- [17] I.A. Buyonava, W.M. Chen, A. Henry, W.-X. Ni, G.V. Hansson, B. Monemar, Phys. Rev. B 52 (1995) 12006.
- [18] H. Weman, B. Monemar, G.S. Oehrlein, S.J. Jeng, Phys. Rev. B 42 (1990) 3109.
- [19] D.K. Sadana, N.H. Norcott, R.G. Wilson, U. Dahmen, Appl. Phys. Lett. 49 (1986) 1169.
- [20] C. Ortiz, J.J. Grob, D. Mathiot, A. Claverie, C. Dubois, R. Jerisian, Nucl. Instr. Methods B 147 (1999) 122.
- [21] N. Arai, S. Takeda, M. Kohyama, Phys. Rev. Lett. 78 (1997) 4265.